Solid-state NMR molecular snapshots of *Aspergillus fumigatus* cell wall architecture during a conidial morphotype transition

Gaëlle Lamon[a] [ID], Alons Lends[a], Isabel Valsecchi[b], Sarah Sze Wah Wong[c], Vincent Duprès[d], Frank Lafont[d], James Tolchard[a], Christine Schmitt[e], Adeline Mallet[e], Axelle Grélard[a] [ID], Estelle Morvan[f], Erick J. Dufourc[a], Birgit Habenstein[a] [ID], J. Iñaki Guijarro[b], Vishukumar Aimanianda[c,1] [ID], and Antoine Loquet[a,1] [ID]

While establishing an invasive infection, the dormant conidia of *Aspergillus fumigatus* transit through swollen and germinating stages, to form hyphae. During this morphotype transition, the conidial cell wall undergoes dynamic remodeling, which poses challenges to the host immune system and antifungal drugs. However, such cell wall reorganization during conidial germination has not been studied so far. Here, we explored the molecular rearrangement of *Aspergillus fumigatus* cell wall polysaccharides during different stages of germination. We took advantage of magic-angle spinning NMR to investigate the cell wall polysaccharides, without employing any destructive method for sample preparation. The breaking of dormancy was associated with a significant change in the molar ratio between the major polysaccharides β-1,3-glucan and α-1,3-glucan, while chitin remained equally abundant. The use of various polarization transfers allowed the detection of rigid and mobile polysaccharides; the appearance of mobile galactosaminogalactan was a molecular hallmark of germinating conidia. We also report for the first time highly abundant triglyceride lipids in the mobile matrix of conidial cell walls. Water to polysaccharides polarization transfers revealed an increased surface exposure of glucans during germination, while chitin remained embedded deeper in the cell wall, suggesting a molecular compensation mechanism to keep the cell wall rigidity. We complement the NMR analysis with confocal and atomic force microscopies to explore the role of melanin and RodA hydrophobin on the dormant conidial surface. Exemplified here using *Aspergillus fumigatus* as a model, our approach provides a powerful tool to decipher the molecular remodeling of fungal cell walls during their morphotype switching.

Aspergillus fumigatus | solid-state NMR | conidium | germination | cell wall dynamics

Aspergillosis encompasses a broad range of diseases ranging from noninvasive allergic bronchopulmonary aspergillosis (ABPA) to invasive aspergillosis (IA). Despite new advances in the diagnosis and the treatment of IA, the morbidity rate (~300,000 cases each year) and mortality (30 to 80%) due to IA remains significantly high, especially for immunocompromised patients (1, 2). Among the 250 species belonging to the genus *Aspergillus*, ~20 species are pathogenic (3), with *Aspergillus fumigatus* being the most commonly isolated species from patients suffering from IA (57%) (4). Due to a limited number of antifungal drugs available for clinical treatment (2, 5) and the emergence of drug resistance (6), *Aspergillus fumigatus* is still highly recalcitrant to most antifungal strategies.

Conidia are microscopic (2 to 3 μm) airborne asexual spores produced by *Aspergillus fumigatus* to restart the fungal life cycle by germination after finding an appropriate environment (7, 8); these conidia are the infectious morphotype. Germination is a characteristic morphological transition starting from dormant conidia (dorC) and leading to the formation of hyphae that constitute the mycelia. Once the dormancy is broken, conidial intracellular osmotic pressure increases causing a quick uptake of water (9, 10). The resulting swollen conidia (swoC) grows isotropically and doubles in cellular diameter as compared to dorC (11, 12). Subsequent polarized growth (gerC) leads to the formation of a germ tube, representing the first stage of hyphal development.

The fungal cell wall constitutes 20 to 40% of the dry cell weight and is mainly composed of different polysaccharides (accounting for >90% of the cell wall content) (13). Whilst the cell wall provides mechanical strength and protects fungal cells, it has the potential to be an ideal antifungal target as the constituent polysaccharides are not found in humans, and its biosynthesis as well as the organization are purely extracellular phenomena (14). In *Aspergillus fumigatus*, the fibrillar cell wall structure is composed mainly of β-1,3-glucan and chitin, whereas the amorphous constituents are α-1,3-glucan and galactomannan (15). In the dormant morphotype, the cell wall polysaccharides are covered by a melanin pigment layer

Significance

Aspergillus fumigatus is an airborne fungal pathogen, which causes fatal invasive infection in immunocompromised hosts. During its life cycle, conidium undergoes morphotype transition from dormant, swollen to germinating stages. In this study, solid-state NMR reveals the conidial cell wall evolution during germination. We show a reshuffling at the level of the glucan composition and in the molecular organization, and we document the behavior of glucans, chitin, and galactosaminogalactan at different growth stages. The advantage in our approach is that an intact fungus could be analyzed without losing the structural details of its cell wall, contrary to other biophysical techniques that require cell wall destruction and derivatization.

and a superficial rodlet layer composed of the hydrophobin RodA protein (16). The rodlet layer confers a hydrophobic coating, facilitating conidial dispersal in air and preventing conidial recognition by the host immune system (17, 18).

So far, the polysaccharide composition of the fungal cell wall has been mainly accessed through semidestructive analytical approaches (15, 19–22). The protocol involves the disintegration of fungal cells to separate the cell wall fractions, removal of associated membrane fractions and proteins from the cell wall fraction, alkali-fractionation of the cell wall, quantification of polysaccharide content by chromatography techniques (23) and their structural elucidation by mass spectrometry (24) and/or solution NMR (25, 26). Nondisruptive techniques based on high-resolution magic-angle spinning (MAS) solid-state NMR spectroscopy have been developed to study polysaccharides in cell walls. Notably, a methodology based on multidimensional MAS NMR was pioneered by Mei Hong, who characterized plant cell walls at atomic resolution (27, 28). Nowadays, such techniques constitute powerful analytical approaches and have been applied to investigate the molecular organization of various samples, ranging from plants (29), algae (30), and fungi (31–33) to bacterial peptidoglycan (34, 35) or cell wall (36–38). Recently, MAS NMR was employed to characterize *Aspergillus fumigatus* mycelial cell wall, that is the cell wall of the fungus in its vegetative state (39, 40). However, while restarting the life cycle or establishing an invasive infection, dorC pass through a germinating morphotype via a swollen stage, before forming hyphae. A detailed molecular picture of the cell wall remodeling during the germination process is still elusive. Indeed, how these morphological changes precisely impact polysaccharide composition, mobility, and surface exposure remain unknown but could be important factors for understanding and potentially targeting nascent fungal infections.

Here, we investigated the molecular organization of dormant, swollen, and germinating *Aspergillus fumigatus* conidia (dorC, swoC, and gerC, respectively). Using MAS NMR, we reveal significant changes at the level of polysaccharide composition between dorC, swoC, and gerC. NMR polarization transfers were employed to distinguish polysaccharides of different mobilities. Water-to-polysaccharide polarization transfer demonstrated that morphological changes have a significant impact on the surface accessibility of cell wall polysaccharides. Overall, our study indicates that the *Aspergillus fumigatus* cell wall undergoes profound compositional changes and remodeling during the germination process.

Results

Aspergillus fumigatus Morphotypes and Their Fixation.
To investigate the molecular organization of *Aspergillus fumigatus* conidial cell wall by MAS NMR, we produced $^{13}C/^{15}N$ labeled conidia by culturing *Aspergillus fumigatus* on agar medium containing ^{13}C-glucose and $^{15}NH_4Cl$ as main carbon and nitrogen sources, respectively, supplemented with salts and trace elements (41). This isotope labeling allowed us to perform high-sensitivity multidimensional MAS NMR. To generate conidia in different growth stages, dorC harvested from agar slants were inoculated into *Aspergillus* Minimal Medium (42) containing ^{13}C-glucose (1%) and $^{15}NH_4Cl$ (20 mM) supplemented with salts and trace elements and incubated at 37 °C under shaking (250 rpm) for 5 h and 8 h, respectively, to obtain swollen (swoC) and germinating (gerC) conidia. Scanning electron microscope images (Fig. 1) showed the surface structures and sizes of conidia in the three stages. Compared to dorC, swoC and gerC were bigger and the germ tube in gerC was smoother than its conidial head. We investigated
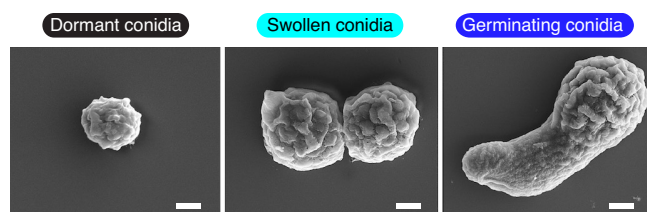

Fig. 1. *Aspergillus fumigatus* conidial morphotypes investigated in this study. Scanning electron microscope images of dormant (dorC), swollen (swoC), and germinating (gerC) conidia (scale bars, 1 μm).

the effect of conidial fixation with *p*-formaldehyde (PFA) on its cell wall integrity by one-dimensional (1D) ^{13}C-detected cross-polarization (CP) experiments (*SI Appendix*, Fig. S1A). Both PFA-fixed and unfixed dorC showed comparable spectral fingerprints, suggesting that the fixation of conidial morphotypes with PFA is a suitable strategy to arrest *Aspergillus fumigatus* growth at a specific stage.

The Rigid Polysaccharides in the *Aspergillus fumigatus* Dormant Conidial Cell Wall. Polysaccharides and other polymeric molecules in the cell wall matrices show a broad range of molecular motions. To investigate the chemical nature and the molecular composition of *Aspergillus fumigatus* dorC, we measured multidimensional MAS NMR experiments using CP-based transfers to enhance signals arising from rigid molecules (rigid on the nanosecond time scale). With short mixing time ^{13}C proton-driven spin-diffusion [PDSD (43)] two-dimensional (2D) $^{13}C-^{13}C$ correlation experiments (Fig. 2A), cross-peaks encode for intramolecular proximities within the rigid biopolymers of the cell wall (27). Well-resolved NMR signals were detected, that allowed a high-resolution study of the cell wall composition. We employed a connectivity-based assignment process to determine the chemical shifts of three biopolymers, α-1,3-glucan, β-1,3-glucan, and chitin. These three polysaccharides were assigned based on the connectivity patterns and by comparison with previous studies (39, 44–46). Fig. 2B displays the chemical structure and experimental chemical shifts. α-1,3-glucan and β-1,3-glucan could be distinguished based on their anomeric C1 chemical shifts, at ~103 ppm and ~106 ppm, respectively. Chitin C2 had a typical up-field resonance due to the covalently bonded acetyl amine group at ~57 ppm.

The ^{13}C line widths in the direct dimension were ~130 Hz on average. Such low values are indicative of a high degree of local structural homogeneity and are comparable to those reported in the literature for similar systems (47). It can hence be deduced that α-1,3-glucan, β-1,3-glucan, and chitin provide a rigid and well-structured scaffold to the cell wall in the dorC morphotype. We note that ^{13}C chemical shift multiplicity is observed for α-1,3-glucan, evidencing polymorphism (*SI Appendix*, Table S1). The relative amount of each polysaccharide was tracked by comparing cross-peak integrals. We established the molar fraction of rigid polysaccharides (Fig. 2D) detected in the PDSD experiment to be approximately 67%, 21%, and 12% (± ~5%), for β-1,3-glucan, α-1,3-glucan, and chitin, respectively.

Although the 2D 50 ms PDSD experiment provides clear connectivity patterns for the above three polysaccharides, spectral ambiguities for ^{13}C sites of similar chemical shifts are possible. Therefore, we conducted a 2D INADEQUATE (48) experiment based on an initial ^1H to ^{13}C CP transfer (i.e., CP-INADEQUATE) to probe rigid biopolymers. The use of a double-quantum dimension is particularly useful to avoid diagonal peaks. The resulting 2D CP-INADEQUATE spectrum (Fig. 2C and *SI Appendix*,
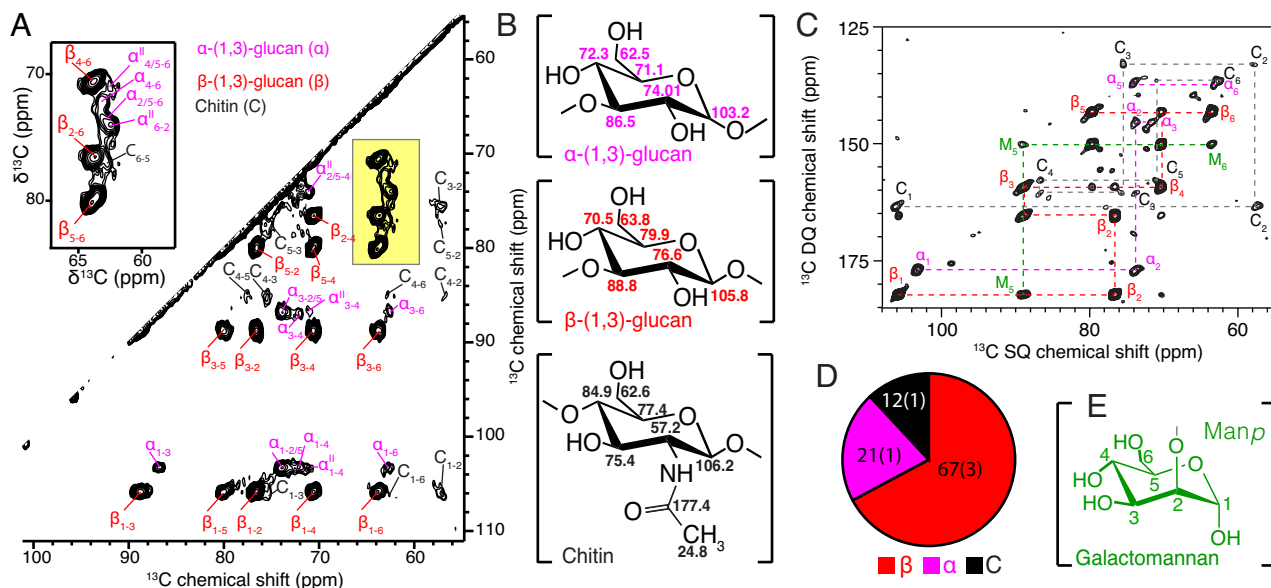
Fig. 2. Characterization of the rigid *Aspergillus fumigatus* conidial cell wall by MAS NMR and identification of polysaccharides. (*A*) 2D 50 ms PDSD spectrum ^{13}C–^{13}C correlation spectrum (^{13}C Larmor frequency of 150 MHz) of *Aspergillus fumigatus* dorC. (*B*) Representative structure of the three main carbohydrates in the cell wall. ^{13}C chemical shifts are indicated. (*C*) 2D CP-INADEQUATE spectrum of *Aspergillus fumigatus* dorC. Abbreviations used for assignments: C for chitin, α for α-1,3-glucan, β for β-1,3-glucan, and M for mannose (galactomannan). (*D*) Estimation of the rigid polysaccharide composition based on NMR peak intensities in PDSD spectra. SEs are shown showed in parentheses. (*E*) Representative structure of galactomannan, showing the terminal mannose unit. The structure of galactomannan is shown in *SI Appendix*, Fig. S1*B*.

Fig. S1B) showed most intramolecular correlations observed in the 2D PDSD experiment, with additional contributions. We identified a new spin system as an α-1,6-mannan unit (structure shown in Fig. 2*E*), which is part of galactomannan (49) (β-1,5-galacto-α-1,2/-α-1,6-mannan), based on comparison with previous literature on synthetic oligosaccharides (50). Galactomannan (*SI Appendix*, *Fig. S1C*) is bound covalently to β-1,3-glucan and possibly to chitin (15) in the insoluble cell wall fraction, while it is also present in the alkali-soluble fraction (51). Two additional minor spin systems of lower intensity were observed (*SI Appendix*, *Fig. S1B*), for which an unambiguous molecular assignment was not possible. Chemical shifts observed for the spin system named Y could be tentatively assigned to a β-galactofuranose unit based on its hexose topology, absence of acetylation, and chemical shifts reported in the literature (52). Galactofuranose is known to be part of galactomannan chains (49). Of note, the length of the O-linked oligosaccharide chain of galactomannan can vary, depending on the culture conditions (53). We note that due to the presence of these minor polysaccharides, the estimation of the molar ratio for the three main polysaccharides might be slightly overestimated.

Mobile Lipids and Polysaccharides in *Aspergillus fumigatus* dorC. To enhance NMR signals arising from mobile molecular components, we employed ^{13}C direct polarization (DP). A 2D DP-INADEQUATE spectrum (Fig. 3*A* and *SI Appendix*, Fig. S2) revealed mobile molecular species of the dorC cell wall. The experiment showed a strong contribution of sharp ^{13}C signals in the region 20 to 60 ppm and 120 to 180 ppm. ^{13}C–^{13}C connectivity patterns indicate a typical lipid spin system associated with an aliphatic acyl chain (spectral region 20 to 40 ppm), a ^{13}C–^{13}C unsaturation (~130 ppm), carbonyl signals (~180 ppm), and two –CH_2–O– signals. This pattern points to the identification of triacylglycerol (TAG) with two glycerol moieties of different electronic environments, at 64.7 and 67.4 ppm (Fig. 3*B*). The 2D DP-INADEQUATE experiment led to a nearly complete ^{13}C–^{13}C through-bond connectivity walk along the TAG molecule,

only stopped by an oxygen between the glycerol and the acyl chain. To corroborate this finding, we analyzed a soluble TAG sample by solution NMR and simulated a pseudo 2D ^{13}C–^{13}C DP-INADEQUATE spectrum to support the solid-state NMR assignment (*SI Appendix*, *Fig. S2C*). Although TAG has not been so far reported as a main contributor to *Aspergillus fumigatus* conidial cell wall composition, recent NMR data indicated its presence in *Cryptococcus neoformans* (32) and also in *Aspergillus niger* (54). The spectral region 60 to 100 ppm was populated with numerous signals, corresponding to other mobile polysaccharides and possibly lipids and glycolipids; however, the spectral crowding limited a precise identification.

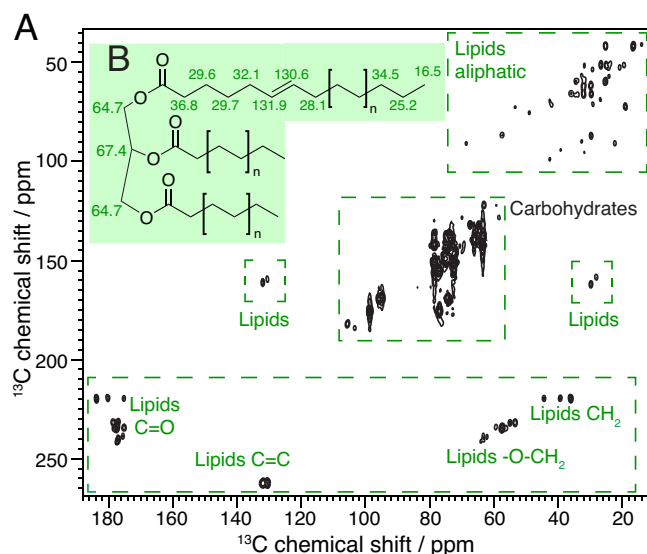**Fig. 3.** Identification of triglycerides in *Aspergillus fumigatus* conidia by MAS NMR. (*A*) 2D DP-INADEQUATE spectrum (^{13}C Larmor frequency of 150 MHz) of *Aspergillus fumigatus* dorC. (*B*) Representative structure of TAG (triacylglycerol).

Molecular Remodeling of the Cell Wall during the Germination Process. To obtain a molecular dissection of the cell wall reshuffling during the germination process, we compared MAS NMR data recorded on three morphotypes of *Aspergillus fumigatus*: dormant (dorC), swollen (swoC), and germinating (gerC) conidia. We first focused on the mobile polysaccharide fraction since the comparison of 2D ^{13}C–^{13}C DP-INADEQUATE spectra showed strong differences (Fig. 4). A new spin system was observed in gerC compared to dorC, with ^{13}C contributions at 109, 84, and 78 ppm (Fig. 4A). We identified it as galactosaminogalactan based on the connectivity patterns suggesting a beta-pyranose linked at the C1 position, no acetyl, or NH$_2$ group linked to the C2 position and by comparison to previous studies (55). Galactosaminogalactan is a linear but heterogeneous polymer composed of galactopyranose (in contrast to galactofuranose found in galactomannan) and *N*-acetyl-galactosamine/galactosamine linked through α-1,4 linkages (56) (Fig. 4B). This polymer is involved in the pathogenesis of aspergillosis (15, 57, 58), by suppressing host inflammatory responses through the masking of α-glucans. Our analysis indicates that galactosaminogalactan is not observed in the rigid or mobile fractions of the dorC cell wall but is predominantly present in the mobile fraction of the gerC cell wall. By comparing galactosaminogalactan signal intensity to that of other polysaccharides, we determined that its molar fraction represents ~25% of the mobile polysaccharides in the gerC cell wall. 1D ^{13}C traces showed the signals of galactosaminogalactan also in swoC, but with a fivefold lower relative abundance compared to gerC (Fig. 4C and *SI Appendix*, Fig. S3). This is in agreement with the expression of genes in the coregulated cluster involved in the biosynthesis of galactosaminogalactan: of the five genes in this cluster, four are not expressed in dorC and start to be expressed when dorC undergo isodiametric swelling (i.e., in swoC).

To further examine cell wall remodeling at the level of rigid polysaccharides, we recorded and compared 2D ^{13}C–^{13}C experiments between the three morphotypes (Fig. 5). The three correlation spectra showed identical polysaccharide patterns, made of α-1,3-glucan, β-1,3-glucan, and chitin correlations, indicating that the chemical nature of rigid polysaccharides in dorC, swoC, and gerC is conserved. However, the relative signal intensities showed significant changes between the three morphotypes, as exemplified with dorC versus gerC (Fig. 5A and *SI Appendix*, Fig. S4) and dorC versus swoC spectra (Fig. 5B), showing that germination has a profound impact on the relative amounts of rigid polysaccharides (Fig. 5C). The glucan composition in the rigid fraction of the dormant state (dorC) was dominated by β-1,3-glucan, with a relative amount of ~67% compared to

α-1,3-glucan (21%). 2D ^{13}C–^{13}C experiment on swoC revealed a significant increase of α-1,3-glucan, by a factor of ~two, representing 41% and a decrease in β-1,3-glucan to ~47%. The changes in composition indicate that once the dormancy is broken, a considerable reshuffling is required at the level of the rigid cell wall to reach the swollen conidial stage, this rearrangement being achieved through a drastic change of the glucan composition. Interestingly, α-1,3-glucan and β-1,3-glucan detected in germinating conidia (gerC) showed an almost identical distribution to dorC, with ~63% and ~25%, respectively. Consequently, although the cell wall glucan composition strongly evolves during germination, it does not follow a homogeneous trend, as we observed highly different α-1,3-glucan (increase) and β-1,3-glucan (decrease) levels during the intermediate swelling stage, compared to the similar levels in first (dormant) and final germinating stages. Interestingly, the relative chitin amount is constant between dorC, swoC, and gerC, with a molar fraction of ~12%. We note that ^{13}C linewidths are comparable between the three morphotypes (Fig. 5D), suggesting that the local structural polymorphism of rigid polysaccharides is not affected by the morphological changes associated with the germination process. Taken together, these results suggest a germination mechanism that substantially influences the glucan composition at the level of the rigid cell wall, while maintaining a constant relative amount of chitin, as well as a conservation of the structural order of the polysaccharide organization.

Chitin in *Aspergillus fumigatus* mycelium (39, 59), *Cryptococcus neoformans* (32), and *Cryptococcus gattii* (60) shows various degrees of local structural polymorphism. This prompted us to employ additional MAS NMR ^{15}N–^{13}C correlation experiments to further investigate the chitin organization in the different conidial morphotypes of *Aspergillus fumigatus*. Because chitin contains a nitrogenous moiety, multidimensional MAS NMR experiments correlating ^{15}N to ^{13}C nuclei offer a suitable strategy to study the molecular polymorphism through the use of selective spectral editing. The presence of chitin is confirmed by a strong amide signal at ~120 ppm observed in a 1D ^{15}N CP experiment (*SI Appendix*, Fig. S5A). A minor contribution was observed at ~32 ppm, and it was assigned to the amine signal of chitosan (*SI Appendix*, Fig. S5B), a deacetylated derivative of chitin (61), often observed in fungal species (62). Chitosan has different physicochemical properties compared to chitin (63) and has putatively the ability to modulate the cell wall integrity (64).

Then, we carried out 2D ^{15}N–^{13}C experiments using an initial ^{1}H to ^{15}N CP followed by a specific double CP (65) between ^{15}N to ^{13}C nuclei to reveal rigid chitinous species through the detection of NH-C2 and NH-CO correlations (Fig. 5E). The spectra

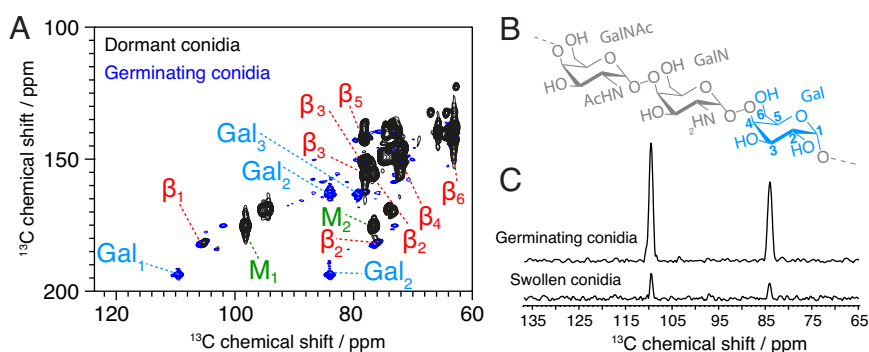**Fig. 4.** Detection of galactosaminogalactan by MAS NMR in swollen and germinating conidia. (*A*) A spectral region for polysaccharides of 2D DP-INADEQUATE spectrum of *Aspergillus fumigatus* dorC (in black) and gerC (in blue) (^{13}C Larmor frequency of 150 MHz). (*B*) Representative structure of galactosaminogalactan. (*C*) 1D ^{13}C traces showing the signals of galactosaminogalactan in swollen and germinating conidia.
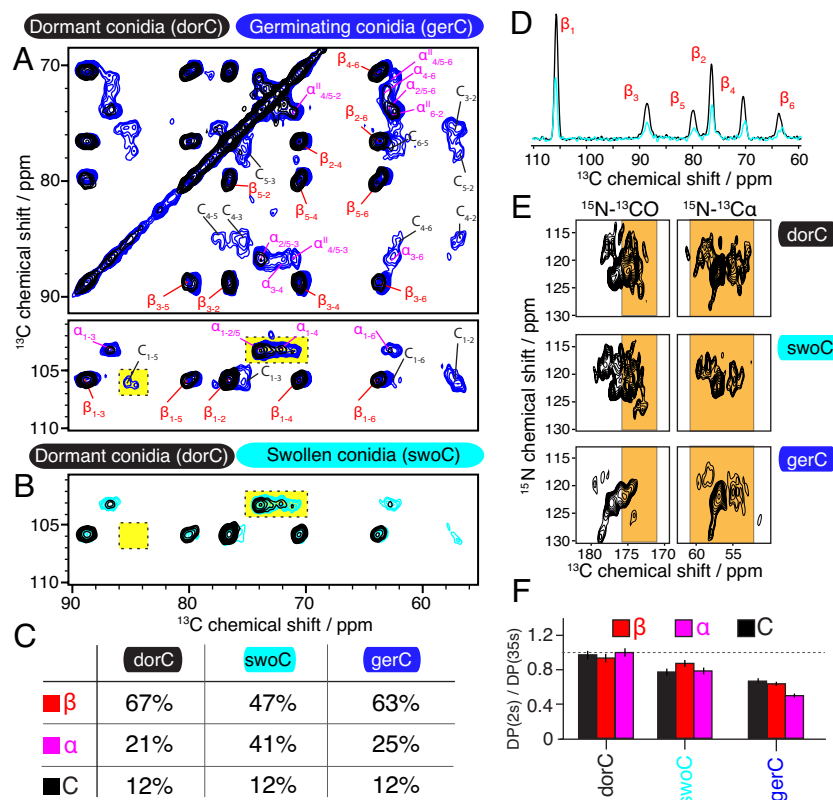
Fig. 5. Polysaccharide composition study of dormant, swollen, and germinating *Aspergillus fumigatus* conidia revealed by MAS NMR. (*A*) Overlay of 2D MAS NMR ^{13}C–^{13}C spectra (^{13}C Larmor frequency of 150 MHz) of *Aspergillus fumigatus* dorC (in black) with gerC (in blue) and (*B*) of dorC (in black) with swoC (in cyan). (*C*) Estimation of the rigid polysaccharide composition in dorC, swoC, and gerC, based on NMR peak intensity. (*D*) 1D ^{13}C traces extracted from 2D data at β-glucan C_1 frequency. As the chitin amount is constant between the three samples, the intensity of the chitin CH_3 signals were first matched, and the other peak intensities were scaled accordingly. (*E*) Comparison of 2D ^{15}N-^{13}C correlation spectra of dorC, swoC, and gerC; the ^{13}C spectral region corresponding to chitinous species is highlighted in orange, based on the results reported earlier (39). (*F*) Peak intensity ratios determined between DP spectra recorded with recycle delays of 2 and 35 s.

contained numerous signals, showing the presence of several chitin subtypes revealed by different chemical shifts. We estimated the number of chitin subtypes to be ~5 to 10. Interestingly, the level of chitin polymorphism differed in the conidial stages, with slightly less polymorphism in gerC. In a previous study on a mycelium sample of *Aspergillus fumigatus* (39), the range of chitin ^{13}C chemical shift was reported to be ~48 to 57 ppm for C2 and 171 to 176 ppm for CO carbons. These chemical shift ranges are highlighted in orange in Fig. 5*E*. Strikingly, the CO chemical shifts detected for the three conidial morphotypes showed a noticeable additional contribution between 175 and 179 ppm, which is a typical range for protein carbonyl signals. This observation is in line with the detection of minor signals in the 1D ^{15}N CP (*SI Appendix*, Fig. S5*A*) at 75 to 85 ppm, where arginine side chain ^{15}N signals are usually detected. Thus, the presence of N-CA (~48 to 57 ppm) and N-CO (175 to 179 ppm) protein backbone signals in the 2D ^{15}N–^{13}C experiment cannot be ruled out, especially considering that 30 to 50% of the dry weight of the cell wall corresponds to proteinaceous content (66). Together, our data indicate a strong tendency of chitin to undergo structural polymorphism in the three conidial morphotypes of *Aspergillus fumigatus*, albeit to a lesser extent in germinating conidia.

We note that the detection of chitosan in the 1D ^{15}N experiment can be exploited to derive the so-called degree of chitin deacetylation, using the ratio between chitin and chitosan intensities (67). We determine a degree of deacetylation of ~1 to 2%, a value observed for the three conidial stages. Nevertheless, the presence of ^{15}N protein signals, as revealed by 2D ^{15}N–^{13}C experiments, might compromise an accurate extraction of this value.

Because the 2D ^{13}C–^{13}C correlation experiments used to derive the polysaccharide molar fractions use an initial CP step, this analysis reveals the fraction of the rigid polysaccharide pool. To complement this analysis and probe the mobile pool of the cell wall, we derived information on polysaccharides associated with high mobility by extracting the intensity ratio between ^{13}C direct pulse experiments using two different recycle delays, namely 2 s and 35 s, following the approach proposed by Tang and coworkers (39). A recycle delay of 35 s favors a quantitative detection, considering that this delay is much longer than ^{13}C longitudinal relaxation T_1 values (*SI Appendix*, Fig. S6), while a short recycle delay of 2 s favors the detection of mobile molecules. DP (2s) / DP (35s) ratios for chitin, α-1,3-glucan, and β-1,3-glucan are presented in Fig. 5*F*. A general trend is observed with a decrease of the DP ratio through the germination process, suggesting an overall decrease of the mobility of polysaccharides.

We hypothesize that the observed stiffening of the cell wall polysaccharide network (decrease of overall mobility in swoC and gerC) could arise from compensatory mechanisms of the mold to cope with the exposure of the polysaccharides upon the disruption of the hydrophobic rodlets/melanin outer layers during germination.

Bulk Water–Polysaccharide Interactions. The surface of dormant *Aspergillus fumigatus* conidium is surrounded by protective layers, mainly composed of melanin (68, 69) and of the hydrophobic protein RodA (18, 70), that prevent conidium from being recognized by the host immune system (71, 72). Because these protective layers disintegrate once conidia start to swell and

germinate (73), we further investigated the water accessibility of cell wall polysaccharides by MAS NMR (Fig. 6). To this end, we recorded two 2D ^{1}H-^{13}C heteronuclear (HETCOR) experiments (74–76), one with a standard pulse sequence and one with an additional water edition sequence, namely, a ^{1}H T_2 filter to suppress the polysaccharide magnetization and keep the bulk water magnetization, followed by a ^{1}H–^{1}H mixing to transfer magnetization from water to the polysaccharides and a final ^{1}H–^{13}C CP to detect on the ^{13}C dimension. A strong contribution at a ^{1}H frequency of ~5 ppm, corresponding to the water ^{1}H resonance, appears in the water-edited HETCOR experiment (highlighted in yellow in Fig. 6A). To establish the mobility of water molecules that contribute to the latter water signal, we measured ^{1}H line widths for dorC, swoC, and gerC samples of ~100 Hz for the three samples (Fig. 6B), indicating that these water molecules are not as dynamic as bulk water, because bulk water would have led to a much narrower ^{1}H line width, as observed for protein samples (5 to 20 Hz) (77). Our observation of less dynamic water molecules interacting with polysaccharides is consistent with ^{1}H line widths previously reported by Hong and coworkers on an intact plant cell wall sample (28). Finally, the similar water ^{1}H line widths displayed by dorC, swoC, and gerC suggest that the morphological evolution of *Aspergillus fumigatus* conidia during the germination process is not associated with a significant change of water mobility at the cell surface.

The spin diffusion exchange in the HETCOR experiment mainly relies on water–polysaccharide proximity and water mobility (28), this later being reflected by the ^{1}H line width, which is effectively the same for the three conidial morphotypes. We note that the exact nature of water–polysaccharide magnetization pathways can be diverse and complex (chemical exchange, dipolar-mediated mechanisms, nuclear Overhauser effects), and further studies following MAS NMR approaches developed for protein samples (e.g., refs. 78 and 79 would help to understand these pathways).

Water-edited experiments can be used to extrapolate the information on water–carbohydrate proximity. Note that because the experiment transfers the ^{1}H magnetization to ^{13}C nuclei using a CP step, it is designed to specifically detect rigid polysaccharides according to their water accessibility. To characterize the polysaccharide content proximal to water, we extracted 1D ^{13}C traces at the water frequency to examine signals of α-1,3-glucan, β-1,3-glucan, and chitin for each conidial morphotype (Fig. 6C and *SI Appendix*, Fig. S7). The water accessibility of α-1,3-glucan and β-1,3-glucan increased during the evolution from dormant to germinating stages. We speculate that this trend is directly related to the macroscopic change of the conidia morphology along the germination process: indeed, the surface loses its hydrophobic layer once the spores swell and germinate, thus leaving the two glucan polysaccharides more exposed to the surface environment. This trend is not observed for chitin, which is slightly less water accessible during germination (vide infra).

To corroborate these observations, we measured water-edited buildup curves by varying the length of the ^{1}H–^{1}H water-to-polysaccharide mixing time. The ^{13}C signal intensity was plotted against the square root of the mixing time to consider the spin diffusion and its associated dipolar-mediated relayed transfers (80). Buildup curves (Fig. 6D) for dorC, swoC, and gerC showed a similar sigmoidal behavior, with a slow initial buildup, followed by a fast-exponential regime and a plateau. DorC and swoC showed a similar trend, with the three polysaccharides having comparable buildup curves, and 50% of the full magnetization recovered at ~10 ms. Since chitin is much less exposed at the conidial surface (81), its contribution in the water-edited experiment implies that the magnetization transfer from the water molecules might have been relayed by an indirect polarization pathway, i.e., via the network of ^{1}H–^{1}H dipolar couplings created by rigid glucans. A similar observation was reported to explain the water-edited signals of crystalline cellulose in the plant cell wall (28). For the germinating conidial stage, we noticed a striking difference for chitin with a slower build-up and 50% of the full magnetization reached at ~22 ms. Thus, the transition between swollen to germinating conidia is associated with a noticeable change in the chitin organization. Altogether, these results point toward a rearrangement of the cell wall polysaccharide organization during the germination process, with chitin undergoing the most important relocalization between the swollen and the germinating stages. It suggests that to maintain the integrity of the germinating conidia, i) chitin might be rearranged to be more
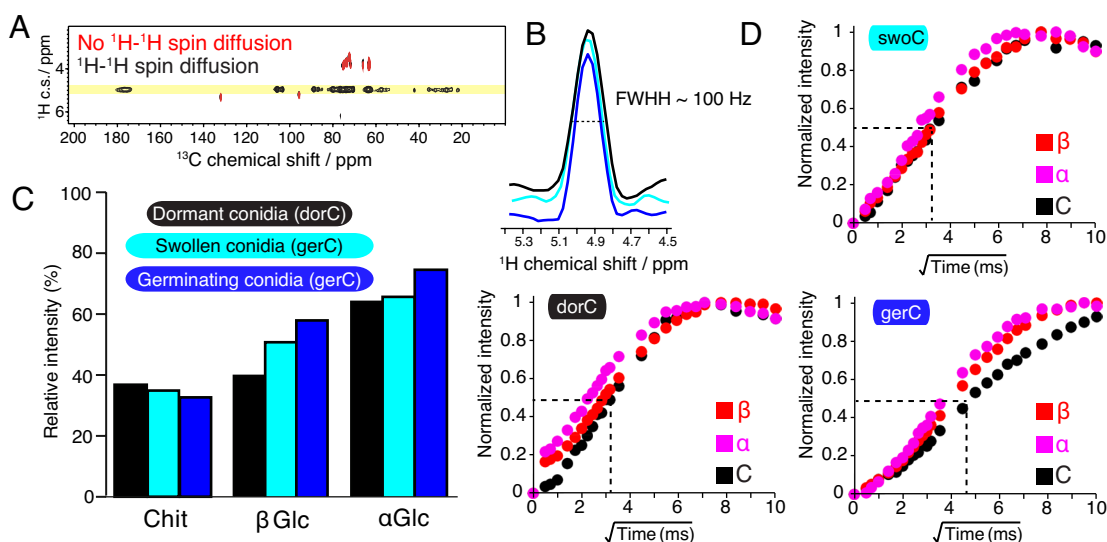

Fig. 6. Water-accessibility of polysaccharides and molecular reshuffling of *Aspergillus fumigatus* conidia. (*A*) 2D MAS NMR 2D correlation ^{1}H-^{13}C HETCOR recorded on *Aspergillus fumigatus* dorC without (in red) and with (in black) water-edition. The spectral region corresponding to ^{1}H water frequency is highlighted in yellow. (*B*) 1D ^{1}H spectra of dorC, swoC, and gerC. Water ^{1}H full width at half height is ~100 Hz. (*C*) Comparison (ratios) of HETCOR versus CP ^{13}C signal intensities expressed as percentage for dorC, swoC, and gerC. (*D*) Water–polysaccharide spin diffusion buildup curves of chitin, α-1,3-glucan, and β-1,3-glucan in dorC, swoC, and gerC.

embedded within the cell wall, interacting less with exposed glucans; or alternatively ii) the glucan layer is more compact, decreasing the accessibility of chitin to the surface environment. Protected chitin will thus act as a structural scaffold when the polarized growth starts. To verify this hypothesis, we probed the localization of chitin in the gerC cell wall by confocal microscopy (*SI Appendix*, Fig. S8) using the lectin wheat-germ agglutinin (WGA) that specifically binds N-acetyl-glucosamine (the building block of chitin) and with Calcofluor White (a small molecule that recognize chitin and can penetrate the fungal cell wall). We had earlier shown by atomic force microscopy that dorC randomly expose ~2 to 8% WGA adhesive structures (82). While in this study, the confocal images of gerC indicate that i) when labeled with WGA, for surface-exposed chitin, only conidial head and germ-tube tips showed positive fluorescence and ii) immunolabeling for β-1,3-glucan (with a specific antibody) and staining chitin with Calcofluor White (a small molecule that can penetrate the fungal cell wall) indicated that in the gerC, chitin is embedded in the β-1,3-glucan layer. Together with MAS NMR data, these data point to a reduced chitin surface exposure in the germinating stage.

RodA Assembly and Interaction with Polysaccharides in dorC. The outer layer of dorC is coated by an additional surface component made of DHN-melanin (1,8-dihydronaphtalene melanin) and rodlet assemblies of the RodA protein. In contrast to the main polysaccharides of the cell wall, MAS NMR experiments did not contain strong protein signals that could be unambiguously assigned to RodA. Moreover, a careful inspection of NMR ^{13}C spectra in the spectral region 110 to 150 ppm, identified by Stark and coworkers (83) as the chemical shift range for melanin in *Cryptococcus neoformans*, was unsuccessful to identify additional connectivity patterns that could be assigned to melanin spin systems. We hypothesize that the low abundance of the melanin pigment in the cell wall compared to polysaccharides, also reported for *Cryptococcus neoformans* (84), could lead to signals beyond NMR detection.

Previous experiments with *Aspergillus fumigatus* mutants deficient in melanin had suggested that this pigment was important for RodA rodlet organization at the conidial surface (85). As deletion mutants lacking cell wall components tend to compensate the lack of a constituent, thus modifying the architecture of the cell wall, we tested if recombinant soluble monomeric RodA could

self-assemble into rodlets at the surface of dorC on which RodA was removed by acid treatment, and on dorC melanin ghosts (dorC devoid of the intracellular milieu, membrane, cell wall polysaccharides, and proteins). Binding of RodA monomers to conidia and melanin ghosts was observed by confocal microscopy using anti-RodA antibodies (Fig. 7 *A–F*). Confocal microscopy indicated that RodA, when added to acid-treated dorC (A,B), to a Δ*rodA* mutant (C,D), and to melanin ghosts (E,F), can indeed interact and cover conidia or melanin ghosts. The formation of RodA rodlets on melanin ghosts was confirmed by AFM (Fig. 7*G*). Further, we investigated by atomic force microscopy (AFM) rodlet formation upon RodA protein interactions with a synthetic analog of DHN-melanin (sMel). AFM micrographs of sMel dried on hydrophilic mica surface did not show any regular structural organization (Fig. 7*H*). In contrast, RodA monomers self-assembled into short independent rodlets (Fig. 7*I*) lacking the lateral association that is observed on the spore surface. On the other hand, when soluble RodA was added to mica surface already covered with sMel, the protein formed well-organized interwoven rodlets structures (Fig. 7*J*), similar to that seen on the surface of *Aspergillus fumigatus* conidia. Together, these results indicate that RodA rodlets interact with melanin in the surface of dorC. We also studied the interaction of exogenous recombinant RodA protein with different conidial morphotypes (*SI Appendix*, Fig. S9). Probing dorC with polyclonal anti-RodA antibodies showed punctate labeling, as in our previous study (85), indicating that the epitopes recognized by the antibodies are not presented uniformly. Preincubation of dorC with recombinant RodA protein followed by probing with anti-RodA antibodies did not intensify labeling, suggesting that preformed rodlets do not back the stacking of additional rodlet layers. On the other hand, swoC and gerC conidia preincubated with RodA protein and probed with anti-RodA antibodies showed negative immunolabeling, suggesting that the exposed components on these two conidial morphotypes do not support rodlet formation.

Discussion

In this work, we have demonstrated the potential of MAS NMR approaches to assess the molecular composition and estimate the molar fraction of the cell wall components of *Aspergillus fumigatus*
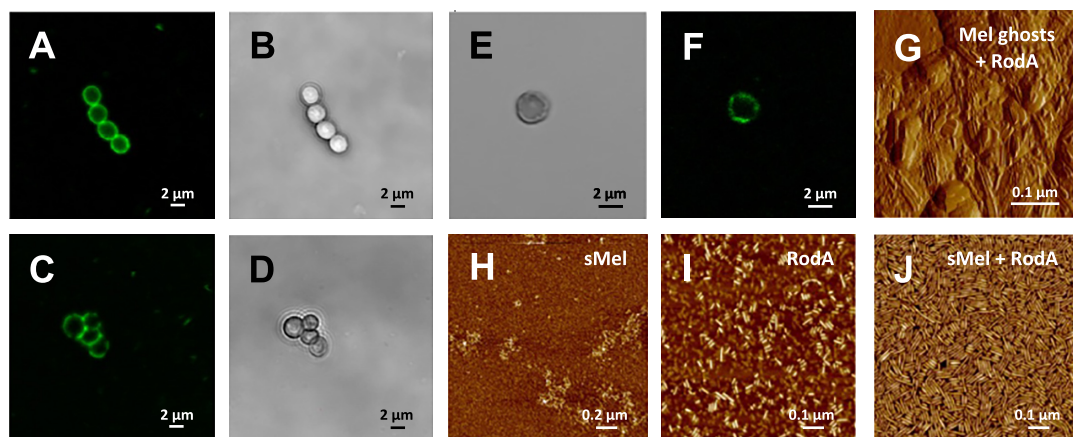

Fig. 7. Binding of recombinant RodA to different conidial surfaces and melanin. Binding of recombinant RodA to (*A* and *B*) dorC parental conidia chemically depleted of RodA by formic acid treatment, (*C* and *D*) dorC of a Δ*rodA* mutant, and (*E* and *F*) dorC melanin ghosts followed by confocal microscopy. RodA was revealed by anti-RodA polyclonal antibodies and FITC-labeled anti-mouse IgG-Alexa fluor 488 antibodies in (*A, C,* and *E*); (*B, D,* and *F*) show the corresponding bright-field images. AFM image of the surface of (*G*) a melanin ghost displaying RodA rodlets after addition of soluble recombinant RodA. AFM analysis of the interaction of RodA with a synthetic analog of DHN-melanin (sMel): (*H*) sMel and (*I*) RodA deposited and dried, respectively, on mica surfaces; (*J*) RodA deposited and dried on a mica surface priorly covered with sMel.

at different growth stages, without employing destructive protocols for fungal sample preparation. The three relevant conidial stages (dorC, swoC, and gerC) were examined, and Fig. 8 depicts a schematic representation of the cell wall evolution between dormant (Fig. 8A) and germinating (Fig. 8B) conidia. We found that the first (isodiametric swelling phase) and second (germ-tube formation) dormant-to-germination transition are associated with a profound molecular reorganization of the cell wall with important variations of the relative amounts of the two rigid major cell wall polysaccharides, α-1,3-glucan and β-1,3-glucan, in the intermediate swollen stage relative to dorC and gerC (Fig. 8C). In dorC, the molar ratio of rigid cell wall polysaccharides were in line with previous data obtained by destructive biochemical methods. On the other hand, while a previous study on mycelia (40) reported, respectively, 50%, 42%, and 8% for these polysaccharides, our data show substantial differences for the main three polysaccharides between the infectious (germinating conidia, i.e., 63%, 25%, and 12%, respectively) and postinfectious (mycelia) stages.

β-1,3-glucan is the major structural polysaccharide component of the cell wall conferring rigidity and turgor pressure resistance and has been targeted for drug development (5, 86). Our data indicate that the dorC to swoC transition is associated with a change of this glucan organization, with a decrease in level from 67% to 46% during transition. This is in agreement with the finding that *Aspergillus fumigatus* morphogenesis requires softening of its cell wall (87). Indeed, transcriptomic analysis during the exit of conidial dormancy indicated downregulation of glycosyl-hydrolase involved in the degradation of cell wall polysaccharide, suggesting that these transcripts are translated into enzymatic proteins to execute their functions during the conidial swelling process (88). We also observed a concomitant doubling of the amount of α-1,3-glucan during the swelling transition. This glucan is not linked to other components in the cell wall (21), thus it suggests that its increase during swelling could compensate for the decrease in the β-1,3-glucan level without affecting the cell wall softening. On the other hand, both these glucans show a similar trend in water-edited experiments in both dorC and swoC stages, with an overall increase in their water accessibility. Our results suggest that in dorC, α-1,3-glucan and β-1,3-glucan are localized in the inner cell wall and partially protected from the external environment by RodA rodlets, with β-1,3-glucan known to have a higher propensity to form rigid polymers than α-1,3-glucan acting as a structural scaffold. Upon swelling, conidia undergo an important transition with the disruption of the RodA layer that interacts with melanin, leading to a higher water accessibility of both glucan polymers. β-1,3-glucan accessibility is most impacted by the rodlet disruption, an observation in line with an earlier study (89) that linked β-1,3-glucan to inflammatory response, advocating for the higher surface exposure of β-1,3-glucan during conidial swelling.

Conidial exit from dormancy to the swollen stage occurs in ~4 to 5 h, and two to three additional hours are required to reach the gerC stage (12). The time range depends on the environmental conditions in which these morphological transitions take place; in nutrient-rich media, the germination rate is faster than in poor nutrient conditions. Atomic force microscopy has demonstrated that within 3 h of growth, the *Aspergillus fumigatus* dormant conidial surface composed of ordered rodlet structures changes into an amorphous material, suggesting that in fungal cell walls, reorganization is a process occurring within hours (90). In support of this observation, the cell wall β-1,3-glucan shows growth stage-specific exposure: it is not exposed on the dormant conidial surface, its exposure is highest on swollen conidia, germinating conidia show discontinuous exposure and its exposure declines in the hyphal morphotype (89).

Our data indicate several changes of the cell wall organization in the transition from the swollen to the germinating phase that leads to the formation of a germ tube through a polarized growth. First, at the level of the composition of the main polysaccharides,
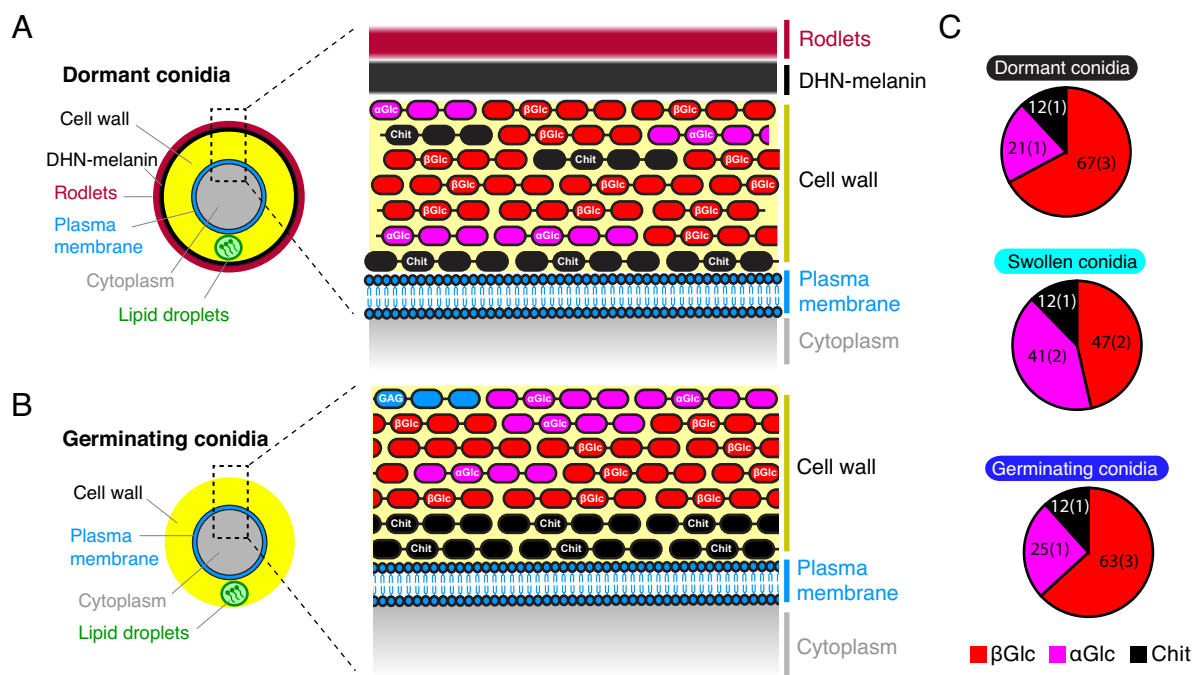

Fig. 8. Schematic representation of *Aspergillus fumigatus* cell surface organization. (A) Spores in the dorC stage. Thickness of layers is not representative but has been set up to illustrate the data. Chitin, α-1,3-glucan, β-1,3-glucan, and galactosaminogalactan are, respectively, shown in the cell wall in green, black, magenta, red, and blue. (B) Spores in the germinating conidial stage, where melanin and the rodA layer are missing. (C) Estimation of the rigid polysaccharide composition based on NMR data for *Aspergillus fumigatus* dorC, swoC, and gerC. SEs are showed in parentheses.

their molar ratios in gerC are comparable to those in dorC but different than in swoC. This could reflect a transient requirement of the swoC that doubles its size on a short time interval, that disappears in the germinating morphotype, which achieves a more stable cell wall composition. We also observed the appearance of galactosaminogalactan as a compositional signature of germinating conidia. This polysaccharide has been previously identified as a major polymer found in the *Aspergillus fumigatus* extracellular matrix, which glues together hyphae at their surface (57, 91). Our data indicate that galactosaminogalactan is observed in the mobile fraction of the cell wall, suggesting its presence in the outer cell wall layer. We do not observe galactosaminogalactan in the rigid inner cell wall by MAS NMR, and we hypothesize that the newly produced galactosaminogalactan in the germinating stage might therefore be more mobile and exposed than α-1,3-glucan/β-1,3-glucan. This observation agrees with previous studies suggesting that recognition of β-1,3-glucan exposure by dectin-1 is decreased in the germinating stage (92). The experimental observation of mobile galactosaminogalactan in gerC by MAS NMR indeed suggests that this polymer could have the capacity to mask β-1,3-glucan upon the dissolution of the rodlets. The estimation of the molar fraction between swoC and gerC indicates an increase of rigid β-1,3-glucan in the germinating stage, that could be interpreted by a rather protective nature of galactosaminogalactan toward β-1,3-glucan at the surface of germinating conidia. This observation corroborates previous immunofluorescence studies showing that the production of galactosaminogalactan by hyphae could induce a reduced exposure of β-1,3-glucan and a subsequent reduction in the inflammatory response (91). It is interesting to note that although galactosaminogalactan might provide a functional "masking" of the glucans in the germinating stage, the surface accessibility for α-1,3-/β-1,3-glucans in gerC is still higher than in swoC as measured by water-edited MAS NMR experiments. From a structural point of view, it suggests that the masking of glucans by galactosaminogalactan in the germinating conidia is not equivalent to that provided by the RodA rodlet layer in dorC.

Albeit in lower proportion, we also found galactosaminogalactan in the cell wall of swoC. This is in accordance with the expression of genes involved in galactosaminogalactan biosynthesis. Indeed, in *Aspergillus fumigatus*, a coregulated cluster of five genes is involved in the galactosaminogalactan biosynthesis (93). As shown by RNAseq, four of these genes are not expressed in dorC; they begin to be expressed after 4 h of conidial incubation in a growth medium [i.e., starting from swoC (94)]. Biochemical analysis by gas-chromatography did not detect galactosaminogalactan in the cell wall of dorC, and immunolabeling with monoclonal anti-galactosaminogalactan antibodies showed positive labeling for swoC/gerC, but not for dorC, clearly suggesting that the biosynthesis of galactosaminogalactan is associated with germination. Galactosaminogalactan is a dominant adhesin synthesized by *Aspergillus fumigatus*; it mediates *Aspergillus fumigatus* hyphal adherence to materials including plastic, fibronectin, and epithelial cells (91)**.** Thus, the hydrophobicity conveyed by the RodA rodlet layer in dorC facilitates conidial dispersal through air, whereas the biosynthesis of the galactosaminogalactan adhesin during germination possibly facilitates hyphal adherence to organic matter favoring saprophytic/infectious growth of *Aspergillus fumigatus*.

Our analysis reveals the presence of intense lipid signals in the cell wall, and we demonstrate that multidimensional MAS NMR experiments provide an efficient approach to chemically characterize the nature of these lipids without semi-destructive lipidomic analysis. We identified triacylglycerol (TAG) to be the main lipid in the cell wall of *Aspergillus fumigatus*. Triacylglycerol is an important source of energy (95) and has been linked to the process of

germination in *Magnaporthe grisea* (96); however, its role in *Aspergillus fumigatus* germination is still unclear. The observation of TAGs in *Aspergillus fumigatus* conidia is interesting since these lipids have been described as potential candidates to be associated with DOPA-melanin in *Cryptococcus neoformans* (60); DHN-melanin is also present in *Aspergillus fumigatus* conidia. We show that TAGs keep a high degree of molecular mobility because we observed the corresponding signals in the DP-INADEQUATE spectrum. TAGs are neutral lipids that can accumulate into a phospholipid monolayer to form lipid droplets (97, 98) due to their poor solubility in phospholipid bilayers. We hypothesize that the experimentally observed TAGs are located in lipid droplets of the conidial cell wall. By undergoing enough molecular mobility in the context of lipid droplets, TAG signals can be selectively filtered using dynamic-based MAS NMR experiments and therefore be observed in the DP-INADEQUATE experiment. A similar observation was reported by Stark and Casadevall for TAGs in *Cryptococcus neoformans* (60), that also kept a high degree of mobility when whole cells were analyzed. A *Saccharomyces cerevisiae* mutant lacking TAG biosynthetic capacity showed defects in its spore cell wall, suggesting that TAGs could be important for cell wall construction (99). On the other hand, fatty acids, the constituents of TAGs, play a role in signal transduction (100). Whether the TAGs we identified in the *Aspergillus fumigatus* cell wall have any such role needs to be examined.

The molar ratio of chitin is constant through the germination process. However, we show here that the structural diversity of chitin species is high in dorC and during germination as revealed by the range of chemical shifts of chitin signals in all three stages. A similar observation was made on a mycelial morphotype of *Aspergillus fumigatus* by Wang et al. (59). Interestingly, we showed that chitin has a different behavior in MAS NMR water-edited experiments compared to glucans, with a noticeable reduction of its surface water accessibility in the germinating stage. We hypothesize that this molecular reshuffling of chitin is intimately associated with the reorganization of glucan. In germinating conidia, the presence of galactosaminogalactan increases the proportion of rigid β-1,3-glucan in the inner cell wall where chitin is also located and the decreased chitin accessibility could be seen as an indirect effect of the more compact glucan organization. We do not exclude that chitin might also undergo specific rearrangement within the inner cell wall during the swoC to gerC transition, to keep the integrity of germinating conidia. Chitin is relatively less accessible than β-1,3-glucan; its relocation to the inner cell wall could confer more protection to the gerC compared to swoC that has a softened cell wall (39, 87).

Though the low amount of surface proteins and the sensitivity limits of MAS NMR have prohibited an efficient characterization of protein signals in this study, the detection of protein assemblies such as RodA rodlets coated to the surface will be of great interest to further investigate protein–polysaccharides interplay. We envision that (dynamic nuclear polarization) DNP-enhanced MAS NMR (101) will offer a promising approach to selectively target signals of surface-accessible proteins (102). Moreover, also not investigated in our study, the molecular structure of *Aspergillus fumigatus* melanin pigments is still a matter of debate. Further experiments, requiring different metabolic isotope labeling and MAS NMR as proposed by Stark and Casadevall for *Cryptococcus neoformans* melanin ghosts (103, 104) would be required to tackle this challenge.

The experimental approach using MAS NMR presented in this study to characterize the cell wall of *Aspergillus fumigatus* conidial morphotypes offers a powerful analytical tool to investigate the molecular changes of fungal cell walls through essential life cycle events such as germination. Moreover, nondestructive sample preparation in this

technique offers an advantage over destructive biochemical methods of fungal cell wall analysis by i) preserving intact cell wall architecture and ii) reducing the duration of the analysis, as biochemical protocols require extraction and derivatization of the cell wall components (15, 105). The ability to analyze the molecular rearrangements of fungal cell walls during the essential life cycle should be valuable to gain better knowledge on the cell wall arrangement and in the development of drugs that target cell wall components.

Materials and Methods

More experimental details can be found in *SI Appendix*.

Preparation of Fungal Samples and Material. The clinical isolate CBS144-89 was streaked on 2% malt-agar slant, incubated at 37 °C overnight and then at ambient temperature for 10 to 12 d. Conidia were collected from this slant using 0.5% aqueous Tween-80 and subcultured on 2% agar slant containing ^{13}C-glucose (1%) and ^{15}NH$_4$Cl (5 mM) and supplemented with salt solution and trace elements; this subculture was maintained at 37 °C overnight and then at ambient temperature for 15 to 18 d. Conidia were harvested from this slant to obtain dorC. To prepare swollen and germinating conidia, dorC were inoculated into liquid *Aspergillus* minimal medium composed of ^{13}C-glucose (1%) and ^{15}NH$_4$Cl (5 mM) and incubated at 37 °C in a shaking incubator maintained at 250 rpm for 5 h (to obtain swoC) and 8 h (for gerC).

MAS NMR Spectroscopy. All MAS NMR experiments were performed on a 14.1 T NMR spectrometer (Bruker Biospin) using 3.2-mm or 4-mm HCN MAS probes.

AFM Analysis. Experiments were performed at room temperature using a Multimode 8 AFM (Bruker). For melanin ghosts imaging, the experiments were performed in liquid using contact mode and oxide-sharpened microfabricated silicon nitride (Si$_3$N$_4$) AFM probes with triangular cantilevers of nominal spring constant of 0.01 N/m (MSCT, Bruker). For recombinant RodA imaging, the experiments were done in air using the ScanAsyst mode and ScanAsyst air AFM probes with a nominal spring constant of 0.4 N/m (Bruker).

Data, Materials, and Software Availability. All study data are included in the article and/or *SI Appendix*.

Author affiliations: [a]Univ. Bordeaux, Centre National de la Recherche Scientifique (CNRS), Bordeaux Institut National Polytechnique, Chemistry and Biology of Membranes and Nanoobjects (CBMN), Unité Mixte de Recherche (UMR) 5248, Institut Européen de Chimie et Biologie (IECB), Pessac F-33607, France; [b]Institut Pasteur, Université de Paris Cité, CNRS, UMR3528, Biological NMR and HDX-MS Platform, Paris, F-75015, France; [c]Institut Pasteur, Université de Paris Cité, CNRS UMR2000, Unité Mycologie Moléculaire, Paris F-75015, France; [d]Univ Lille, CNRS, INSERM, Centre Hospitalier Universitaire (CHU) Lille, Institut Pasteur de Lille, Center for Infection and Immunity of Lille, Lille F-59000, France; [e]Institut Pasteur, Institut Pasteur, Ultrastructural Bioimaging Unit F-75015, Paris, France; and [f]Univ. Bordeaux, CNRS, INSERM, IECB, Unité d'Appui et de la Recherche (UAR) 3033, Pessac F-33607, France

1. J. W. Baddley *et al.*, Factors associated with mortality in transplant patients with invasive Aspergillosis. *Clin. Infect. Dis.* **50**, 1559–1567 (2010).
2. F. Bongomin, S. Gago, R. O. Oladele, D. W. Denning, Global and multi-national prevalence of fungal diseases–estimate precision. *J. Fungi* **3**, 57 (2017).
3. S. A. Balajee *et al.*, Aspergillus species identification in the clinical setting. *Stud. Mycol.* **59**, 39–46 (2007).
4. J. Cadena, G. R. Thompson, T. F. Patterson, Invasive Aspergillosis: Current strategies for diagnosis and management. *Infect. Dis. Clin. North Am.* **30**, 125–142 (2016).
5. L. Ostrosky-Zeichner, A. Casadevall, J. N. Galgiani, F. C. Odds, J. H. Rex, An insight into the antifungal pipeline: selected new molecules and beyond. *Nat. Rev. Drug Discov.* **9**, 719–727 (2010).
6. N. Robbins, T. Caplan, L. E. Cowen, Molecular evolution of antifungal drug resistance. *Annu. Rev. Microbiol.* **71**, 753–775 (2017).
7. J. P. Latgé, Aspergillus fumigatus and aspergillosis. *Clin. Microbiol. Rev.* **12**, 310–350 (1999).
8. T. J. H. Baltussen, J. Zoll, P. E. Verweij, W. J. G. Melchers, Molecular mechanisms of conidial germination in *Aspergillus* spp. *Microbiol. Mol. Biol. Rev.* **84**, e00049–19 (2020).
9. A. Taubitz, B. Bauer, J. Heesemann, F. Ebel, Role of respiration in the germination process of the pathogenic mold Aspergillus fumigatus. *Curr. Microbiol.* **54**, 354 (2007).
10. M. R. V. Leeuwen, T. M. V. Doorn, E. A. Golovina, J. Stark, J. Dijksterhuis, Water- and air-distributed conidia differ in sterol content and cytoplasmic microviscosity. *Appl. Environ. Microb.* **76**, 366–369 (2010).
11. M. R. van Leeuwen *et al.*, Germination of conidia of Aspergillus niger is accompanied by major changes in RNA profiles. *Stud. Mycol.* **74**, 59–70 (2013).
12. T. J. H. Baltussen, J. P. M. Coolen, J. Zoll, P. E. Verweij, W. J. G. Melchers, Gene co-expression analysis identifies gene clusters associated with isotropic and polarized growth in Aspergillus fumigatus conidia. *Fungal Genet. Biol.* **116**, 62–72 (2018).
13. J.-P. Latgé, The cell wall: a carbohydrate armour for the fungal cell. *Mol. Microbiol.* **66**, 279–290 (2007).
14. V. Aimanianda, J. P. Latgé, Problems and hopes in the development of drugs targeting the fungal cell wall. *Expert Rev. Anti Infect. Ther.* **8**, 359–364 (2010).
15. T. Fontaine *et al.*, Molecular organization of the alkali-insoluble fraction of Aspergillus fumigatus cell wall. *J. Biol. Chem.* **275**, 27594–27607 (2000).
16. A. Gastebois, C. Clavaud, V. Aimanianda, J. P. Latgé, Aspergillus fumigatus: Cell wall polysaccharides, their biosynthesis and organization. *Future Microbiol.* **4**, 583–595 (2009).
17. J. A. Sugui, K. J. Kwon-Chung, P. R. Juvvadi, J.-P. Latgé, W. J. Steinbach, Aspergillus fumigatus and related species. *Cold Spring Harb. Perspect. Med.* **5**, a019786 (2015).
18. V. Aimanianda *et al.*, Surface hydrophobin prevents immune recognition of airborne fungal spores. *Nature* **460**, 1117–1121 (2009).
19. R. Kollár *et al.*, Architecture of the yeast cell wall. Beta(1→6)-glucan interconnects mannoprotein, beta(1→3)-glucan, and chitin. *J. Biol. Chem.* **272**, 17762–17775 (1997).
20. S. M. Bowman, S. J. Free, The structure and synthesis of the fungal cell wall. *Bioessays* **28**, 799–808 (2006).
21. J. P. Latgé, A. Beauvais, G. Chamilos, The cell wall of the human fungal pathogen Aspergillus fumigatus: Biosynthesis, organization, immune response, and virulence. *Annu. Rev. Microbiol.* **71**, 99–116 (2017).
22. J. M. François, A simple method for quantitative determination of polysaccharides in fungal cell walls. *Nat. Protoc.* **1**, 2995–3000 (2006).
23. L. Alvarez, S. B. Hernandez, M. A. de Pedro, F. Cava, Ultra-sensitive, high-resolution liquid chromatography methods for the high-throughput quantitative analysis of bacterial cell wall chemistry and structure. *Methods Mol. Biol.* **1440**, 11–27 (2016).
24. F. A. Pettolino, C. Walsh, G. B. Fincher, A. Bacic, Determining the polysaccharide composition of plant cell walls. *Nat. Protoc.* **7**, 1590–1607 (2012).
25. H. N. Cheng, T. G. Neiss, Solution NMR spectroscopy of food polysaccharides. *Polymer Rev.* **52**, 81–114 (2012).
26. F. Lu, J. Ralph, Non-degradative dissolution and acetylation of ball-milled plant cell walls: high-resolution solution-state NMR. *Plant J.* **35**, 535–544 (2003).
27. M. Pérez García *et al.*, Structure and interactions of plant cell-wall polysaccharides by two- and three-dimensional magic-angle-spinning solid-state NMR. *Biochemistry* **50**, 989–1000 (2011).
28. P. B. White, T. Wang, Y. B. Park, D. J. Cosgrove, M. Hong, Water-polysaccharide interactions in the primary cell wall of Arabidopsis thaliana from polarization transfer solid-state NMR. *J. Am. Chem. Soc.* **136**, 10399–10409 (2014).
29. T. Wang, P. Phyo, M. Hong, Multidimensional solid-state NMR spectroscopy of plant cell walls. *Solid State Nucl. Magn. Reson* **78**, 56–63 (2016).
30. A. Poulhazan *et al.*, Identification and quantification of glycans in whole cells: Architecture of microalgal polysaccharides described by solid-state nuclear magnetic resonance. *J. Am. Chem. Soc.* **143**, 19374–19388 (2021).
31. H. L. Ehren *et al.*, Characterization of the cell wall of a mushroom forming fungus at atomic resolution using solid-state NMR spectroscopy. *Cell Surf.* **6**, 100046 (2020).
32. C. Chrissian *et al.*, Solid-state NMR spectroscopy identifies three classes of lipids in Cryptococcus neoformans melanized cell walls and whole fungal cells. *J. Biol. Chem.* **295**, 15083–15096 (2020).
33. C. Chrissian *et al.*, Unconventional constituents and shared molecular architecture of the melanized cell wall of Cryptococcus neoformans and spore wall of Saccharomyces cerevisiae. *J. Fungi* **6**, 329 (2020).
34. T. Kern *et al.*, Toward the characterization of peptidoglycan structure and protein-peptidoglycan interactions by solid-state NMR spectroscopy. *J. Am. Chem. Soc.* **130**, 5618–5619 (2008).
35. S. J. Kim, J. Chang, M. Singh, Peptidoglycan architecture of Gram-positive bacteria by solid-state NMR. *Biochim. Biophys. Acta* **1848**, 350–362 (2015).
36. M. Renault *et al.*, Cellular solid-state nuclear magnetic resonance spectroscopy. *Proc. Natl. Acad. Sci. U.S.A.* **109**, 4863–4868 (2012).
37. H. Takahashi *et al.*, Solid-state NMR on bacterial cells: Selective cell wall signal enhancement and resolution improvement using dynamic nuclear polarization. *J. Am. Chem. Soc.* **135**, 5105–5110 (2013).
38. R. Nygaard, J. A. H. Romaniuk, D. M. Rice, L. Cegelski, Spectral snapshots of bacterial cell-wall composition and the influence of antibiotics by whole-cell NMR. *Biophys. J.* **108**, 1380–1389 (2015).
39. X. Kang *et al.*, Molecular architecture of fungal cell walls revealed by solid-state NMR. *Nat. Commun.* **9**, 2747 (2018).
40. A. Chakraborty *et al.*, A molecular vision of fungal cell wall organization by functional genomics and solid-state NMR. *Nat. Commun.* **12**, 6346 (2021).

41. A. Gastebois et al., Characterization of a new beta(1–3)-glucan branching activity of Aspergillus fumigatus. *J. Biol. Chem.* **285**, 2386–2396 (2010).

42. T. W. Hill, E. Kafer, Improved protocols for Aspergillus minimal medium: Trace element and minimal medium salt stock solutions. *Fungal Genet. Rep.* **48**, 20–21 (2001).

43. N. M. Szeverenyi, M. J. Sullivan, G. E. Maciel, Observation of spin exchange by two-dimensional Fourier-transform C-13 cross polarization-magic-angle spinning. *J. Magn. Reson.* **47**, 462–475 (1982).

44. S. Hazime, M. Takashi, T. Ryoko, H. Shigehiro, High resolution 13C NMR spectra of chitin oligomers in aqueous solution. *Chem. Lett.* **10**, 1483–1484 (1981).

45. S. Hazime, T. Ryoko, S. Takuma, Y. YŪko, A high-resolution solid-state 13C NMR study of (1→3)-β-D-glucans from various sources. conformational characterization as viewed from the conformation-dependent 13C chemical shifts and its consequence to gelation property. *Bull. Chem. Soc. Japan* **59**, 2093–2101 (1986).

46. S. Hanashima et al., NMR study of short β(1–3)-glucans provides insights into the structure and interaction with Dectin-1. *Glycoconj J.* **31**, 199–207 (2014).

47. N. Ghassemi et al., Solid-state NMR investigations of extracellular matrixes and cell walls of algae, bacteria, fungi, and plants. *Chem. Rev.* **122**, 10036–10086 (2021).

48. A. Lesage, C. Auger, S. Caldarelli, L. Emsley, Determination of through-bond carbon-carbon connectivities in solid-state NMR using the INADEQUATE experiment. *J. Am. Chem. Soc.* **119**, 7867–7868 (1997).

49. J. P. Latgé et al., Chemical and immunological characterization of the extracellular galactomannan of Aspergillus fumigatus. *Infect. Immun.* **62**, 5424–5433 (1994).

50. V. B. Krylov et al., Synthesis of oligosaccharides related to galactomannans from Aspergillus fumigatus and their NMR spectral data. *Organic Biomol. Chem.* **16**, 1188–1199 (2018).

51. J. P. Latge, Galactofuranose containing molecules in Aspergillus fumigatus. *Med. Mycol.* **47**, S104–109 (2009).

52. E. Alexandersson, G. Nestor, Complete 1H and 13C NMR spectral assignment of d-glucofuranose. *Carbohydrate Res.* **511**, 108477 (2022).

53. A. Kudoh, Y. Okawa, N. Shibata, Significant structural change in both O- and N-linked carbohydrate moieties of the antigenic galactomannan from Aspergillus fumigatus grown under different culture conditions. *Glycobiology* **25**, 74–87 (2014).

54. E. V. Morozova, V. P. Kozlov, V. M. Tereshina, A. S. Memorskaia, E. P. Feofilova, Changes in lipid composition and carbohydrate composition of Aspergillus niger conidia during germination. *Prikl. Biokhim. Mikrobiol.* **38**, 149–154 (2002).

55. H. Y. Yao, J. Q. Wang, J. Y. Yin, S. P. Nie, M. Y. Xie, A review of NMR analysis in polysaccharide structure and conformation: Progress, challenge and perspective. *Food Res. Int.* **143**, 110290 (2021).

56. B. Briard, I. Muszkieta, J. P. Latgé, T. Fontaine, Galactosaminogalactan of Aspergillus fumigatus, a bioactive fungal polymer. *Mycologia* **108**, 572–580 (2016).

57. C. Loussert et al., In vivo biofilm composition of Aspergillus fumigatus. *Cell Microbiol.* **12**, 405–410 (2010).

58. A. Beauvais et al., Aspergillus biofilm In vitro and in vivo. *Microbiol. Spectr.* **3** (2015), 10.1128/microbiolspec.MB-0017-2015.

59. L. D. Fernando et al., Structural polymorphism of chitin and chitosan in fungal cell walls from solid-state NMR and principal component analysis. *Front. Mol. Biosci.* **8**, 727053 (2021).

60. C. Chrissian et al., Melanin deposition in two Cryptococcus species depends on cell-wall composition and flexibility. *J. Biol. Chem.* **295**, 1815–1828 (2020).

61. M. Gierszewska, K. Struszczyk-Świta, S. Hudson, "Chitin and chitosan" in *Encyclopedia of Polymer Science and Technology* (John Wiley & Sons, 2022), pp. 1–16.

62. P. Pochanavanich, W. Suntornsuk, Fungal chitosan production and its characterization. *Lett. Appl. Microbiol.* **35**, 17–21 (2002).

63. J. Roy, F. Salaun, A. Ferri, G. Chen, J. Guan, *Solubility of Chitin: Solvents, Solution Behaviors and Their Related Mechanisms* (InTechOpen, London, 2017).

64. I. Mouyna et al., What are the functions of chitin deacetylases in Aspergillus fumigatus? *Front. Cell Infect. Microbiol.* **10**, 28 (2020).

65. M. Baldus, D. G. Geurts, S. Hediger, B. H. Meier, Efficient 15N–13C polarization transfer by adiabatic passage Hartmann-Hahn cross-polarization. *J. Magn. Reson. A* **118**, 140–144 (1996).

66. R. Garcia-Rubio, H. C. de Oliveira, J. Rivera, N. Trevijano-Contador, The fungal cell wall: Candida, cryptococcus, and aspergillus species. *Front. Microbiol.* **10**, 2993 (2020).

67. M. R. Kasaai, Determination of the degree of N-acetylation for chitin and chitosan by various NMR spectroscopy techniques: A review. *Carbohydrate Polymers* **79**, 801–810 (2010).

68. B. Jahn et al., Isolation and characterization of a pigmentless-conidium mutant of Aspergillus fumigatus with altered conidial surface and reduced virulence. *Infect. Immun.* **65**, 5110–5117 (1997).

69. M. Pihet et al., Melanin is an essential component for the integrity of the cell wall of Aspergillus fumigatus conidia. *BMC Microbiol.* **9**, 177 (2009).

70. S. Paris et al., Conidial hydrophobins of Aspergillus fumigatus. *Appl. Environ. Microbiol.* **69**, 1581–1588 (2003).

71. T. Heinekamp et al., Aspergillus fumigatus melanins: Interference with the host endocytosis pathway and impact on virulence. *Front. Microbiol.* **3**, 440 (2013).

72. J. Carrion Sde et al., The RodA hydrophobin on Aspergillus fumigatus spores masks dectin-1- and dectin-2-dependent responses and enhances fungal survival in vivo. *J. Immunol.* **191**, 2581–2588 (2013).

73. I. Valsecchi et al., Assembly and disassembly of Aspergillus fumigatus conidial rodlets. *Cell Surface* **5**, 100023 (2019).

74. K. K. Kumashiro, K. Schmidt-Rohr, L. K. Thompson, A novel tool for probing membrane protein structure: solid-state NMR with proton spin diffusion and X-nucleus detection. *J. Am. Chem. Soc.* **120**, 5043 (1998).

75. C. Ader et al., Structural rearrangements of membrane proteins probed by water-edited solid-state NMR spectroscopy. *J. Am. Chem. Soc.* **131**, 170–176 (2009).

76. W. Luo, M. Hong, Conformational changes of an ion channel detected through water-protein interactions using solid-state NMR spectroscopy. *J. Am. Chem. Soc.* **132**, 2378–2384 (2010).

77. A. Bockmann et al., Characterization of different water pools in solid-state NMR protein samples. *J. Biomol. NMR* **45**, 319–327 (2009).

78. A. Lesage, L. Emsley, F. Penin, A. Bockmann, Investigation of dipolar-mediated water-protein interactions in microcrystalline Crh by solid-state NMR spectroscopy. *J. Am. Chem. Soc.* **128**, 8246–8255 (2006).

79. A. Lesage et al., Polarization transfer over the water-protein interface in solids. *Angew. Chem. Int. Ed. Engl.* **47**, 5851–5854 (2008).

80. K. Schmidt-Rohr, H. W. Spiess, *Multidimensional solid-state NMR and Polymers* (Academic Press, San Diego, 1994).

81. I. Valsecchi et al., The role of RodA-conserved cysteine residues in the Aspergillus fumigatus conidial surface organization. *J. Fungi* **6**, 151 (2020).

82. D. Alsteens et al., Unraveling the nanoscale surface properties of chitin synthase mutants of Aspergillus fumigatus and their biological implications. *Biophys J.* **105**, 320–327 (2013).

83. R. P. Baker, C. Chrissian, R. E. Stark, A. Casadevall, Cryptococcus neoformans melanization incorporates multiple catecholamines to produce polytypic melanin. *J. Biol. Chem.* **298**, 101519 (2022).

84. E. Camacho et al., The structural unit of melanin in the cell wall of the fungal pathogen Cryptococcus neoformans. *J. Biol. Chem.* **294**, 10471–10489 (2019).

85. I. Valsecchi et al., The puzzling construction of the conidial outer layer of Aspergillus fumigatus. *Cell. Microbiol.* **21**, e12994 (2019).

86. D. W. Denning, Echinocandin antifungal drugs. *Lancet* **362**, 1142–1151 (2003).

87. I. Mouyna et al., GH16 and GH81 family β-(1,3)-glucanases in Aspergillus fumigatus are essential for conidial cell wall morphogenesis. *Cell Microbiol.* **18**, 1285–1293 (2016).

88. C. Lamarre et al., Transcriptomic analysis of the exit from dormancy of Aspergillus fumigatus conidia. *BMC Genom.* **9**, 417 (2008).

89. T. M. Hohl et al., Aspergillus fumigatus triggers inflammatory responses by stage-specific beta-glucan display. *PLoS Pathog.* **1**, e30 (2005).

90. E. Dague, D. Alsteens, J. P. Latgé, Y. F. Dufrêne, High-resolution cell surface dynamics of germinating Aspergillus fumigatus conidia. *Biophys J.* **94**, 656–660 (2008).

91. F. N. Gravelat et al., Aspergillus galactosaminogalactan mediates adherence to host constituents and conceals hyphal β-glucan from the immune system. *PLoS pathog.* **9**, e1003575 (2013).

92. C. Steele et al., The beta-glucan receptor dectin-1 recognizes specific morphologies of Aspergillus fumigatus. *PLoS Pathog.* **1**, e42 (2005).

93. C. Speth, G. Rambach, C. Lass-Flörl, P. L. Howell, D. C. Sheppard, Galactosaminogalactan (GAG) and its multiple roles in Aspergillus pathogenesis. *Virulence* **10**, 976–983 (2019).

94. B. Briard et al., Galactosaminogalactan activates the inflammasome to provide host protection. *Nature* **588**, 688–692 (2020).

95. D. Sorger, G. Daum, Triacylglycerol biosynthesis in yeast. *Appl. Microbiol. Biotechnol.* **61**, 289–299 (2003).

96. E. Thines, R. W. Weber, N. J. Talbot, MAP kinase and protein kinase A-dependent mobilization of triacylglycerol and glycogen during appressorium turgor generation by Magnaporthe grisea. *Plant Cell* **12**, 1703–1718 (2000).

97. K. Tauchi-Sato, S. Ozeki, T. Houjou, R. Taguchi, T. Fujimoto, The surface of lipid droplets is a phospholipid monolayer with a unique fatty acid composition. *J. Biol. Chem.* **277**, 44507–44512 (2002).

98. J. A. Olzmann, P. Carvalho, Dynamics and functions of lipid droplets. *Nat. Rev. Mol. Cell Biol.* **20**, 137–155 (2019).

99. T. H. Hsu, R. H. Chen, Y. H. Cheng, C. W. Wang, Lipid droplets are central organelles for meiosis II progression during yeast sporulation. *Mol. Biol. Cell* **28**, 440–451 (2017).

100. R. Rhome, M. Del Poeta, Lipid signaling in pathogenic fungi. *Annu. Rev. Microbiol.* **63**, 119–131 (2009).

101. A. Chakraborty et al., Biomolecular complex viewed by dynamic nuclear polarization solid-state NMR spectroscopy. *Biochem. Soc. Trans.* **48**, 1089–1099 (2020).

102. D. Gauto, O. Dakhlaoui, I. Marin-Montesinos, S. Hediger, G. De Paëpe, Targeted DNP for biomolecular solid-state NMR. *Chem. Sci.* **12**, 6223–6237 (2021).

103. S. Tian, J. Garcia-Rivera, B. Yan, A. Casadevall, R. E. Stark, Unlocking the molecular structure of fungal melanin using 13C biosynthetic labeling and solid-state NMR. *Biochemistry* **42**, 8105–8109 (2003).

104. J. Zhong, S. Frases, H. Wang, A. Casadevall, R. E. Stark, Following fungal melanin biosynthesis with solid-state NMR: biopolymer molecular structures and possible connections to cell-wall polysaccharides. *Biochemistry* **47**, 4701–4710 (2008).

105. N. Shibata, A. Suzuki, H. Kobayashi, Y. Okawa, Chemical structure of the cell-wall mannan of Candida albicans serotype A and its difference in yeast and hyphal forms. *Biochem. J.* **404**, 365–372 (2007).